九州大学学術情報リポジトリ
Kyushu University Institutional Repository

Periodic and Quasi-Periodic Orbit Design based on the Center Manifold Theory

Akiyama, Yuki
Department of Aeronautics and Astronautics, Kyushu University

Bando, Mai
Department of Aeronautics and Astronautics, Kyushu University

Hokamoto, Shinji
Department of Aeronautics and Astronautics, Kyushu University

https://hdl.handle.net/2324/4784354

出版情報：Acta Astronautica. 160, pp.672-682, 2019-07. Elsevier
バージョン：
権利関係：

KYUSHU UNIVERSITY

Periodic and Quasi-Periodic Orbit Design based on the Center Manifold Theory

Yuki Akiyama[a,*], Mai Bando[a], Shinji Hokamoto[a]

[a] *Department of Aeronautics and Astronautics, Kyushu University, 744 Motooka, Nishu-ku, Fukuoka 819-0395, Japan*

Abstract

This paper proposes a new numerical method for finding libration point orbits in the vicinity of collinear libration points in the circular restricted three-body problem. The main advantage of this method is that it requires neither an initial guess nor complex algebraic manipulations for finding both quasi-periodic and periodic orbits. The proposed method consists of two steps: center manifold design and differential correction. The first step provides a quasi-periodic orbit parametrized by a single parameter vector. In the second step, the parameter vector in the first step is used to obtain an exact periodic orbit. This method is applied to find periodic and quasi-periodic orbits in the Sun-Earth restricted three-body problem around the L_1 and L_2 libration points.

Keywords: Center Manifold Theorem, Periodic Orbit, Quasi-Periodic Orbit

1. Introduction

The libration point orbits in the circular restricted three-body problem (CRTBP) have attracted much interest due to their advantageous properties for space missions [1, 2, 3, 4]. There exist five libration points (also referred to as Lagrangian points), and they are derived from geometric relationships [5, 6].

☆Fully documented templates are available in the elsarticle package on CTAN.

*Corresponding author

Email addresses: akimaru@aero.kyushu-u.ac.jp (Yuki Akiyama), mbando@aero.kyushu-u.ac.jp (Mai Bando), hokamoto@aero.kyushu-u.ac.jp (Shinji Hokamoto)

Moreover, there are several types of bounded orbits in the vicinity of the three collinear libration points, referred to as libration point orbits [7, 8, 9, 10, 11, 12]. Lyapunov, vertical, and halo orbits are periodic, while Lissajous and quasi-halo orbits are quasi-periodic. These libration point orbits have associated invariant manifolds that could be stable or unstable. Therefore, it is possible to inject/eject spacecraft into/from a libration point orbit via these manifolds with sufficiently small fuel consumption. Libration point orbits are also considered as the best location for the new generation of formation flying missions [13, 14].

The design of a reference orbit is a primal problem for space missions since an accurate knowledge of the orbit characteristics often results in considerable savings of fuel consumption. According to literature in the field, there are two classical methods to find periodic orbits: the differential correction method and the Lindstedt-Poincaré method. The former is a numerical method including correction procedures based on Newton's method. Howell constructed the numerical determination method by iteratively correcting an initial guess of an initial condition of a libration point orbit, known as single-shooting differential correction [8]. The latter is an analytical method based on perturbation theory. Richardson constructed first- and third-order analytical approximations for libration point orbits by linearizing the equations of motion and showed that the third-order analytical approximation gives trajectories sufficiently close to numerical solutions obtained by differential correction [15]. On the other hand, a number of studies have considered the problem of finding quasi-periodic orbits. Howell and Pernicka introduced a so-called multiple-shooting differential correction that smoothly connects multiple patch points, and they proposed a numerical procedure to numerically generate Lissajous orbits [16]. Koleman et al. presented a fully numerical method that employed multiple Poincaré sections to find quasi-periodic orbits [17]. Olikara et al. proposed methods for computing quasi-periodic invariant tori generated based on a natural parameterization and a continuation scheme [18, 19]. Broschart et al. described the characteristics of the quasi-periodic orbits in the solar radiation pressure perturbed Hill three-body problem [20]. Baresi et al. calculated the invariant tori to compute the

quasi-periodic orbits around an asteroid as an alternative concept for future asteroid exploration missions [21]. However, finding accurate quasi-periodic orbits around the libration points demands more complicated parametrization or computation than finding periodic orbits. The station-keeping strategies for those orbits have also been intensively studied in recent years [22, 23, 24, 25, 26, 27].

Recently, Akiyama et al. proposed a new semi-analytical method to compute a quasi-periodic orbit in the CRTBP [28, 29]. Independently, Nagata et al. proposed the center manifold method for bounded orbits [30]. Both methods above relied on the successive approximation method to calculate center manifolds proposed by Suzuki et al. [31]. Comparing other proposed techniques to obtain bounded orbits, the main advantage of the center manifold method is that all the bounded orbits including quasi-periodic orbits lying on center manifolds are parametrized by a single parameter vector. Furthermore, although quasi-periodic orbitals are obtained in a successive manner, each iteration only needs to solve ordinary differential equations, and our approach does not require selecting the Poincaré section. However, the main drawback is that most of the orbits obtained by this method are quasi-periodic and it cannot be determined in advance whether the obtained orbit is periodic or quasi-periodic.

In this paper, we extend our previous method to obtain periodic orbits in order to overcome the difficulties faced by conventional methods. The advantages of the proposed method are that (1) periodic and quasi-orbits can be easily generated without an initial guess or extensive algebraic manipulations, which are necessary in the conventional methods, being required, and (2) the approach does not require bifurcation analysis to reach solutions that are not predicted from linear analysis. The proposed method includes two steps: center manifold design and differential correction. The first step generates a family of quasi-periodic orbit (possibly periodic orbit) based on the center manifold theory and provides an initial guess for the correction step via center manifold reduction. Then, the differential correction is applied to obtain an exact periodic orbit from the family. To demonstrate the method, results of finding periodic and quasi-periodic orbits in the Sun-Earth restricted three-body problem around L_1

and L_2 libration points are shown.

2. Equations of Motion in the CRTBP

In the CRTBP, the equations of motion in non-dimensional form [32] are expressed as

$$\begin{aligned} X'' - 2Y' &= \frac{\partial U}{\partial X} \\ Y'' + 2X' &= \frac{\partial U}{\partial Y} \\ Z'' &= \frac{\partial U}{\partial Z} \end{aligned} \tag{1}$$

where $\{X, Y, Z\}$ is the rotating frame whose origin is the barycenter of the system, the coordinates and time are normalized by the distance between two main bodies and by the period of the circular orbit, respectively, $(\cdot)'$ denotes the differentiation of $(\cdot)$ with respect to the non-dimensional time t, and

$$\begin{aligned} U &= \frac{1-\mu}{r_1} + \frac{\mu}{r_2} + \frac{1}{2}\left(X^2 + Y^2\right) \\ r_1 &= \sqrt{(X+\mu)^2 + Y^2 + Z^2} \\ r_2 &= \sqrt{(X-1+\mu)^2 + Y^2 + Z^2} \end{aligned}$$

where $\mu = M_2/(M_1 + M_2)$, and M_1 and M_2 are the masses of the two main bodies with $M_1 > M_2$.

Equation (1) has libration points L_i satisfying

$$\frac{\partial U}{\partial X} = \frac{\partial U}{\partial Y} = \frac{\partial U}{\partial Z} = 0 \tag{2}$$

giving

$$\begin{aligned} &L_1 = (l_1(\mu), 0, 0), \quad L_2 = (l_2(\mu), 0, 0), \quad L_3 = (l_3(\mu), 0, 0) \\ &L_4 = (1/2 - \mu, \sqrt{3}/2, 0), \quad L_5 = (1/2 - \mu, -\sqrt{3}/2, 0) \end{aligned}$$

where $l_i(\mu)$ are determined by setting $Y = 0$ and solving $\partial U/\partial X = 0$. To describe the motion near a collinear libration point L_i $(i = 1, 2, 3)$, it is convenient

to use a coordinate system with the origin located at L_i. Replacing $\{X, Y, Z\}$ with $\{x + l_i, y, z\}$ and rewriting Eq. (1) in the state space form yields

$$\boldsymbol{x}' = \boldsymbol{f}(\boldsymbol{x}) \tag{3}$$

where $\boldsymbol{x} = \begin{bmatrix} x & y & z & x' & y' & z' \end{bmatrix}^{\mathrm{T}}$ and

$$\boldsymbol{f}(\boldsymbol{x}) = \begin{bmatrix} x' \\ y' \\ z' \\ \dfrac{\partial U}{\partial x} + 2y' \\ \dfrac{\partial U}{\partial y} - 2x' \\ \dfrac{\partial U}{\partial z} \end{bmatrix} \tag{4}$$

Equation (3) can be divided into a linear term and a nonlinear term as

$$\boldsymbol{x}' = \boldsymbol{A}\boldsymbol{x} + \tilde{\boldsymbol{f}}(\boldsymbol{x}) \tag{5}$$

where

$$\boldsymbol{A} = \left.\frac{\partial \boldsymbol{f}}{\partial \boldsymbol{x}}\right|_{\mathbf{0}} = \begin{bmatrix} 0 & 0 & 0 & 1 & 0 & 0 \\ 0 & 0 & 0 & 0 & 1 & 0 \\ 0 & 0 & 0 & 0 & 0 & 1 \\ 2\sigma_i + 1 & 0 & 0 & 0 & 2 & 0 \\ 0 & 1 - \sigma_i & 0 & -2 & 0 & 0 \\ 0 & 0 & -\sigma_i & 0 & 0 & 0 \end{bmatrix}$$

$$\tilde{\boldsymbol{f}}(\boldsymbol{x}) = \boldsymbol{f}(\boldsymbol{x}) - \boldsymbol{A}\boldsymbol{x}$$

$$\sigma_i = \frac{1 - \mu}{|l_i(\mu) + \mu|^3} + \frac{\mu}{|l_i(\mu) - 1 + \mu|^3}$$

Since computation of a center manifold requires a higher-order nonlinear term, a semi-linear form is useful to develop the procedure of calculation of the center manifold.

The matrix $\boldsymbol{A}$ has four purely imaginary eigenvalues $\pm\lambda_{c_1}, \pm\lambda_{c_2}$, one negative real eigenvalue λ_s, and one positive real eigenvalue $\lambda_u (= -\lambda_s)$. Accordingly,

there exists a four-dimensional center manifold, a one-dimensional stable manifold, and a one-dimensional unstable manifold for each of the collinear libration points. Therefore, Eq. (5) can be transformed to diagonal form by the transformation matrix $\boldsymbol{T}$ given by

$$\boldsymbol{T} = \begin{bmatrix} \mathrm{Re}(\boldsymbol{v}_{c_1}) & \mathrm{Im}(\boldsymbol{v}_{c_1}) & \mathrm{Re}(\boldsymbol{v}_{c_2}) & \mathrm{Im}(\boldsymbol{v}_{c_2}) & \boldsymbol{v}_s & \boldsymbol{v}_u \end{bmatrix} \tag{6}$$

where $\boldsymbol{v}_j$ is the normalized eigenvector corresponding to λ_j $(j = c_1, c_2, s, u)$. The explicit notation of the transformation matrix $\boldsymbol{T}$ is given in Appendix A. The new state vector $\boldsymbol{z} = \begin{bmatrix} z_{c_1} & z_{c_2} & z_{c_3} & z_{c_4} & z_s & z_u \end{bmatrix}^{\mathrm{T}} = \boldsymbol{T}^{-1}\boldsymbol{x}$ is given by

$$\boldsymbol{z} = \begin{bmatrix} \dfrac{\sqrt{1+\sigma_i}}{\sqrt{\sigma_i}} z' \\ \\ -\sqrt{1+\sigma_i} z \\ \\ \dfrac{\Lambda_2 d_2 Q_2}{(d_3 - d_2)(\sigma_i - 1)} \left(\Lambda_3^2 x + d_3 y'\right) \\ \\ -\dfrac{d_2 Q_2}{(d_3 - d_2)} \left(d_3 y + x'\right) \\ \\ -\dfrac{d_3 Q_3}{2(d_3 - d_2)} \left[\dfrac{\Lambda_3}{\sigma_i - 1}\left(\Lambda_2^2 x - d_2 y'\right) - \left(d_2 y + x'\right)\right] \\ \\ -\dfrac{d_3 Q_3}{2(d_3 - d_2)} \left[\dfrac{\Lambda_3}{\sigma_i - 1}\left(\Lambda_2^2 x - d_2 y'\right) + \left(d_2 y + x'\right)\right] \end{bmatrix} \tag{7}$$

The diagonal form of Eq. (5) is expressed as

$$\begin{aligned} \boldsymbol{z}_c' &= \boldsymbol{P}\boldsymbol{z}_c + \boldsymbol{g}_c(\boldsymbol{z}_c, z_s, z_u) \\ z_s' &= Q z_s + g_s(\boldsymbol{z}_c, z_s, z_u) \\ z_u' &= R z_u + g_u(\boldsymbol{z}_c, z_s, z_u) \end{aligned} \tag{8}$$

where $\boldsymbol{z}_c = \begin{bmatrix} z_{c_1} & z_{c_2} & z_{c_3} & z_{c_4} \end{bmatrix}^{\mathrm{T}}$; $(\boldsymbol{z}_c, z_s, z_u) \in \mathbb{R}^4 \times \mathbb{R}^1 \times \mathbb{R}^1$; $\boldsymbol{P}$ is a 4×4 matrix whose eigenvalues are $\pm\lambda_{c_1}, \pm\lambda_{c_2}$, $Q = \lambda_s$, and $R = \lambda_u$; and $\boldsymbol{g}_c$, g_s, and g_u are nonlinear functions.

3. Periodic and Quasi-Periodic Orbit Design

This section introduces a procedure to design periodic and quasi-periodic orbits in the CRTBP. The proposed method consists of two steps: center manifold design step and differential correction. The first step provides a quasi-periodic (possibly periodic) orbit based on the center manifold theory. The second step modifies the orbit obtained by the first step to generate a periodic orbit by applying the differential correction.

3.1. Center manifold design step

To compute the center manifold in the CRTBP, this step is based on the center manifold theorem [33, 34] and the successive approximation method [31]. According to the center manifold theorem, there exist local center manifolds near equilibria that describe the behavior of small bounded solutions. Therefore, if the state $\boldsymbol{z}$ lies on the local center manifold, there exist local center manifolds ψ_1 and ψ_2, and the reduced order system of Eq. (8) can be expressed as

$$\boldsymbol{z}_c{}' = \boldsymbol{P}\boldsymbol{z}_c + \boldsymbol{g}_c\left(\boldsymbol{z}_c, \psi_1\left(\boldsymbol{z}_c\right), \psi_2\left(\boldsymbol{z}_c\right)\right) \tag{9}$$

Furthermore, z_s and z_u are expressed as the function of $\boldsymbol{z}_c$ rather than time as

$$z_s = \psi_1(\boldsymbol{z}_c) \tag{10}$$

$$z_u = \psi_2(\boldsymbol{z}_c) \tag{11}$$

The dimension of the state of the CRTBP is reduced from six to four since the stable and unstable components are constrained by the reduced-order system.

Equation (9) can be transformed into an integral equation with a parameter $\boldsymbol{\xi} = \boldsymbol{z}_c(t_0) \in \mathbb{R}^4$ as

$$\boldsymbol{z}_c\left(t, \boldsymbol{\xi}\right) = e^{\boldsymbol{P}t}\boldsymbol{\xi} + \int_0^t e^{\boldsymbol{P}(t-\tau)}\boldsymbol{g}_c\left(\boldsymbol{z}_c, z_s, z_u\right) d\tau \tag{12}$$

where states $z_s(t, \boldsymbol{\xi})$ and $z_u(t, \boldsymbol{\xi})$ in Eq. (12) can be calculated by solving the following equations from $t = \infty$ and $t = -\infty$, respectively, since $z_s(\infty, \boldsymbol{\xi}) = 0$

and $z_u(-\infty, \boldsymbol{\xi}) = 0$.

$$z_s\left(t, \boldsymbol{\xi}\right) = \int_{-\infty}^{t} e^{Q(t-\tau)} g_s\left(\boldsymbol{z}_c, z_s, z_u\right) d\tau \tag{13}$$

$$z_u\left(t, \boldsymbol{\xi}\right) = \int_{t}^{\infty} e^{R(t-\tau)} g_u\left(\boldsymbol{z}_c, z_s, z_u\right) d\tau \tag{14}$$

The solution to the initial value problem of Eqs. (9), (10), and (11) is found by constructing a sequence of approximation solutions for integral equations Eqs. (12), (13), and (14) recursively. A first approximation of the solution is given by

$$\boldsymbol{z}_{c,0}\left(t, \boldsymbol{\xi}\right) = e^{\boldsymbol{P}t}\boldsymbol{\xi}, \quad z_{s,0}\left(\boldsymbol{z}_{c,0}\left(t, \boldsymbol{\xi}\right)\right) = 0, \quad z_{u,0}\left(\boldsymbol{z}_{c,0}\left(t, \boldsymbol{\xi}\right)\right) = 0 \tag{15}$$

The next step is to use $\boldsymbol{z}_{c,0}$, $z_{s,0}$, and $z_{u,0}$ in Eq. (15) to generate better approximate solutions $\boldsymbol{z}_{c,1}$, $z_{s,1}$, and $z_{u,1}$. The successive approximation method repeats this process, which gives the sequences of functions $\{\boldsymbol{z}_{c,k}\left(t, \boldsymbol{\xi}\right)\}$, $\{z_{s,k}\left(t, \boldsymbol{\xi}\right)\}$ and $\{z_{u,k}\left(t, \boldsymbol{\xi}\right)\}$ from the k-th approximation functions as follows:

$$\begin{aligned}
\boldsymbol{z}_{c,k+1}\left(t, \boldsymbol{\xi}\right) &= e^{\boldsymbol{P}t}\boldsymbol{\xi} + \int_{0}^{t} e^{\boldsymbol{P}(t-\tau)} \boldsymbol{g}_c\left(\boldsymbol{z}_{c,k}, z_{s,k}, z_{u,k}\right) d\tau \\
z_{s,k+1}\left(t, \boldsymbol{\xi}\right) &= \int_{-\infty}^{t} e^{Q(t-\tau)} g_s\left(\boldsymbol{z}_{c,k}, z_{s,k}, z_{u,k}\right) d\tau \\
z_{u,k+1}\left(t, \boldsymbol{\xi}\right) &= \int_{t}^{\infty} e^{R(t-\tau)} g_u\left(\boldsymbol{z}_{c,k}, z_{s,k}, z_{u,k}\right) d\tau \qquad k = 0, 1, 2, \cdots
\end{aligned} \tag{16}$$

The sequences $\{\boldsymbol{z}_{c,k}\left(t, \boldsymbol{\xi}\right)\}$, $\{z_{s,k}\left(t, \boldsymbol{\xi}\right)\}$, and $\{z_{u,k}\left(t, \boldsymbol{\xi}\right)\}$ define the approximations of the exact solution of Eqs. (12), (13), and (14). In addition, these sequences are uniformly convergent to the exact solutions $\{\boldsymbol{z}_c\left(t, \boldsymbol{\xi}\right)\}$, $\{z_s\left(t, \boldsymbol{\xi}\right)\}$, and $\{z_u\left(t, \boldsymbol{\xi}\right)\}$, respectively, as $k \to \infty$. For the CRTBP, applying Eq. (16) yields the approximate solutions of bounded libration point orbits. It should be noted that periodic and quasi-periodic orbits are completely parametrized by the single 4-dimensional parameter vector $\boldsymbol{\xi}$.

In the numerical computation of the center manifold step, the infinite integral in Eq. (16) is replaced by finite time $T_t > 0$, and large amplitude orbits require large T_t to replace the infinite interval by a finite interval. However, a large time interval leads divergence of state variables during the computation due to the

instability of the system. To avoid numerical instability, starting with a small $T_1 < T_t$, the endpoint of the converged solution is used to extend the solution to $T_1 \leq t \leq T_t$. Moreover, this procedure can provide quasi-periodic orbits, such as quasi-vertical, quasi-halo, and Lissajous orbits, with long periods.

3.2. Differential correction step

In the previous section, the new computational method to find quasi-periodic orbits was proposed. This method has the advantage that a single parameter vector $\boldsymbol{\xi}$ uniquely determines the remaining initial states to form a periodic or quasi-periodic orbit. However, it does not give information on whether the obtained orbit is an *exact* periodic orbit or not. Therefore, a modification process to obtain an exact periodic orbit is required. In this process, the solution to the first step is regarded as the initial guess for the differential correction step and corrected to form an exact periodic orbit.

3.2.1. State transition matrix

Let $\boldsymbol{z}_n(t) = \begin{bmatrix} z_{c_1,n}(t) & z_{c_2,n}(t) & z_{c_3,n}(t) & z_{c_4,n}(t) & z_{s,n}(t) & z_{u,n}(t) \end{bmatrix}^{\mathrm{T}}$ be a nominal periodic orbit, and define the variation $\delta\boldsymbol{z}(t) = \boldsymbol{z}(t) - \boldsymbol{z}_n(t)$. The time derivative of the variation is computed as

$$\begin{aligned} \delta\boldsymbol{z}'(t) &= \left(\boldsymbol{D} + \left. \frac{\partial \boldsymbol{g}(\boldsymbol{z}(t))}{\partial \boldsymbol{z}(t)} \right|_{\boldsymbol{z}_n(t)} \right) \delta\boldsymbol{z}(t) \\ &\triangleq \boldsymbol{W}(t)\delta\boldsymbol{z}(t) \end{aligned} \tag{17}$$

where $\boldsymbol{D} = \mathrm{diag}\begin{bmatrix} \boldsymbol{P} & Q & R \end{bmatrix}$ and $\boldsymbol{g} = \begin{bmatrix} \boldsymbol{g}_c^{\mathrm{T}} & g_s & g_u \end{bmatrix}^{\mathrm{T}}$. The solution of Eq. (17) is given by

$$\delta\boldsymbol{z}(t) = \boldsymbol{\Phi}(t, t_0)\delta\boldsymbol{z}(t_0) \tag{18}$$

where $\boldsymbol{\Phi}(t, t_0)$ is the state transition matrix (STM) that satisfies

$$\boldsymbol{\Phi}'(t, t_0) = \boldsymbol{W}(t)\boldsymbol{\Phi}(t, t_0), \quad \boldsymbol{\Phi}(t, t) = \boldsymbol{I} \tag{19}$$

3.2.2. Deviation of initial state

Periodic orbits in the CRTBP are symmetric with respect to the x-z plane. The periodic orbit intersects the x-z plane with only a non-zero velocity component in the y-direction and passes the plane at a time exactly equal to one-half of the period, *i.e.*, $t_c = \frac{1}{2}t_p$, where t_p is the period of periodic orbit. From this observation and Eq. (7), the parameter vector can be set as $\boldsymbol{\xi} = \boldsymbol{z}_c(t_0) = \begin{bmatrix} 0 & z_{c_2}(t_0) & z_{c_3}(t_0) & 0 \end{bmatrix}^{\mathrm{T}}$. This means that the symmetry with respect to the x-z plane corresponds to one with respect to the z_{c_2}-z_{c_3} plane. Then, the state vectors of the nominal orbit at $t = t_0$ and $t = t_c$ are given by

$$\boldsymbol{z}_n(t_0)=\begin{bmatrix} 0 & z_{c_2,n}(t_0) & z_{c_3,n}(t_0) & 0 & z_{s,n}(t_0) & z_{u,n}(t_0) \end{bmatrix}^{\mathrm{T}} \tag{20}$$

$$\boldsymbol{z}_n(t_c)=\begin{bmatrix} 0 & z_{c_2,n}(t_c) & z_{c_3,n}(t_c) & 0 & z_{s,n}(t_c) & z_{u,n}(t_c) \end{bmatrix}^{\mathrm{T}} \tag{21}$$

Similarly, the initial guess of $\boldsymbol{z}_n(t_0)$ and the corresponding state vector at $t = t_c$ are given by

$$\boldsymbol{z}(t_0)=\begin{bmatrix} 0 & z_{c_2}(t_0) & z_{c_3}(t_0) & 0 & z_s(t_0) & z_u(t_0) \end{bmatrix}^{\mathrm{T}} \tag{22}$$

$$\boldsymbol{z}(t_c)=\begin{bmatrix} z_{c_1}(t_c) & z_{c_2}(t_c) & z_{c_3}(t_c) & z_{c_4}(t_c) & z_s(t_c) & z_u(t_c) \end{bmatrix}^{\mathrm{T}} \tag{23}$$

Note that since the period t_p is unknown, t_p or t_c must be obtained along with $\boldsymbol{z}(t_0)$ by the differential correction step. Let $t_{c,n}$ be the half-period of the nominal periodic orbit, and define the deviation of the half-period as $\delta t_c = t_c - t_{c,n}$. Then, the variation $\delta\boldsymbol{z}(t_c) = \boldsymbol{z}(t_c) - \boldsymbol{z}_n(t_c)$ can be computed as

$$\delta\boldsymbol{z}(t_c) = \begin{bmatrix} \boldsymbol{\Phi}(t_c, t_0) & \boldsymbol{z}'(t_c) \end{bmatrix} \begin{bmatrix} \delta\boldsymbol{z}(t_0) \\ \delta t_c \end{bmatrix} \tag{24}$$

The derivation of Eq. (24) is given in Appendix B.

Comparing Eqs. (20)–(23) yields $\delta z_{c_1}(t_0) = \delta z_{c_4}(t_0) = 0$, $\delta z_{c_1}(t_c) = z_{c_1}(t_c)$ and $\delta z_{c_4}(t_c) = z_{c_4}(t_c)$. Thus, one can obtain the deviations by solving Eq. (24)

for $\delta z_{c_1}(t_c)$ and $\delta z_{c_4}(t_c)$:

$$\begin{bmatrix} \delta z_{c_1}(t_c) \\ \delta z_{c_4}(t_c) \end{bmatrix} = \begin{bmatrix} \phi_{12} & \phi_{13} & \phi_{15} & \phi_{16} & z'_{c_1}(t_c) \\ \phi_{42} & \phi_{43} & \phi_{45} & \phi_{46} & z'_{c_4}(t_c) \end{bmatrix} \begin{bmatrix} \delta z_{c_2}(t_0) \\ \delta z_{c_3}(t_0) \\ \delta z_s(t_0) \\ \delta z_u(t_0) \\ \delta t_c \end{bmatrix} \tag{25}$$

where $\delta z_j(t) = z_j(t) - w_{j,n}(t)$ and $\phi_{ij} = \mathbf{\Phi}(t_c, t_0)_{ij}$.

Here, $z_{c_2}(t_0)$, $z_{c_3}(t_0)$, and t_c are considered as design parameters in the process, and we consider two types of corrections for $\boldsymbol{\xi}$: the z_{c_2}-fixed case and the z_{c_3}-fixed case. If $z_{c_2}(t_0)$ is fixed, then $\delta z_{c_2}(t_0) = 0$. The required variations at t_c are $-z_{c_1}(t_c)$ for $\delta z_{c_1}(t_c)$ and $-z_{c_4}(t_c)$ for $\delta z_{c_4}(t_c)$. Hence, from Eq. (25), the initial variations are given by

$$\begin{bmatrix} \delta z_{c_3}(t_0) \\ \delta z_s(t_0) \\ \delta z_u(t_0) \\ \delta t_c \end{bmatrix} = \begin{bmatrix} \phi_{13} & \phi_{15} & \phi_{16} & z'_{c_1}(t_c) \\ \phi_{43} & \phi_{45} & \phi_{46} & z'_{c_4}(t_c) \end{bmatrix}^{-1} \begin{bmatrix} -z_{c_1}(t_c) \\ -z_{c_4}(t_c) \end{bmatrix} \tag{26}$$

Similarly, the initial variations in the z_{c_3}-fixed case are given by

$$\begin{bmatrix} \delta z_{c_2}(t_0) \\ \delta z_s(t_0) \\ \delta z_u(t_0) \\ \delta t_c \end{bmatrix} = \begin{bmatrix} \phi_{12} & \phi_{15} & \phi_{16} & z'_{c_1}(t_c) \\ \phi_{42} & \phi_{45} & \phi_{46} & z'_{c_4}(t_c) \end{bmatrix}^{-1} \begin{bmatrix} -z_{c_1}(t_c) \\ -z_{c_4}(t_c) \end{bmatrix} \tag{27}$$

Equations (26) and (27) include the variations $\delta z_s(t_0)$ and $\delta z_u(t_0)$. However, corrections for $z_s(t_0)$ and $z_u(t_0)$ are not necessary in this process because $z_s(t_0)$ and $z_u(t_0)$ are determined uniquely as functions of $\boldsymbol{z}_c$ in the center manifold design step. By repeating these corrections, the initial state and the crossing time converge to those forming periodic orbits. To clarify these procedures, a flow chart is given in Fig. 1. Moreover, the families of periodic orbits can be computed by numerical continuation technique.

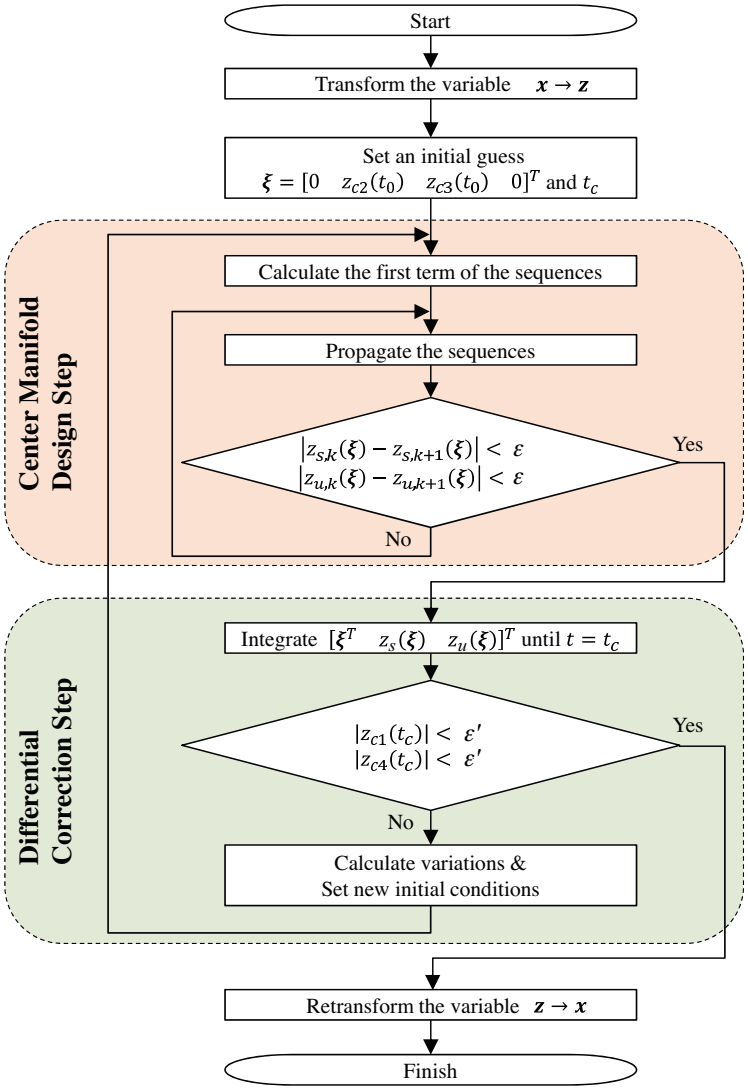

Figure 1: Flow chart of center manifold design method for periodic orbits.

4. Simulations

In this section, the proposed method is applied to find quasi-periodic and periodic orbits in the Sun-Earth system. The period of the Sun-Earth system is $T_0 = 365.25$ days and the radius is $R_0 = 1.4960 \times 10^8$ km, which is the average distance between the Sun and Earth. The origin of the coordinates is fixed at L_1 or L_2. Then, the related parameters are specified as $\mu = 3.0038 \times 10^{-6}$, $l_1 = 0.98997$, $l_2 = 1.0101$, $\sigma_1 = 4.0612$, and $\sigma_2 = 3.9393$. The finite time in the center manifold step is set as $T_t = \pi$. The convergence threshold is $\varepsilon = 1.0 \times 10^{-19}$ for the center manifold design step and $\varepsilon' = 1.0 \times 10^{-12}$ for the differential correction step. All the simulations were performed by MATLAB R2017b on a notebook computer with an Intel Core i7-4800MQ 2.70 GHz processor and 16.0 GB RAM. It should be noted that each iteration step for the center manifold design step took 0.075 seconds on average on the notebook.

4.1. Physical meaning of the parameter vector

All periodic or quasi-periodic orbits lying on the center manifold of the system are parametrized by a single 4-dimensional vector $\boldsymbol{\xi}$. From Eq. (7), only z_{c_1} and z_{c_2} affect the out-of-plane motion. Therefore, planar libration point orbits can be obtained by setting $z_{c_1}(t_0) = z_{c_2}(t_0) = 0$. Otherwise, the orbits converge to three-dimensional periodic or quasi-periodic orbits.

As examples, the libration point orbits are computed by setting one element of the parameter vector to 0.01 and the remainder to 0. The Lagrangian point is fixed at L_1. The orbits obtained by each parameter vector are shown in Figs. 2–4. When either $z_{c_1}(t_0)$ or $z_{c_2}(t_0)$ is nonzero, the obtained orbits are quasi vertical Lyapunov orbits whose amplitudes in the z-direction are much higher than those in the x and y directions (Figs. 2 and 3). On the contrary, the orbits using only $z_{c_3}(t_0)$ or $z_{c_4}(t_0)$ are planar periodic orbits called Lyapunov orbits (Fig. 4).

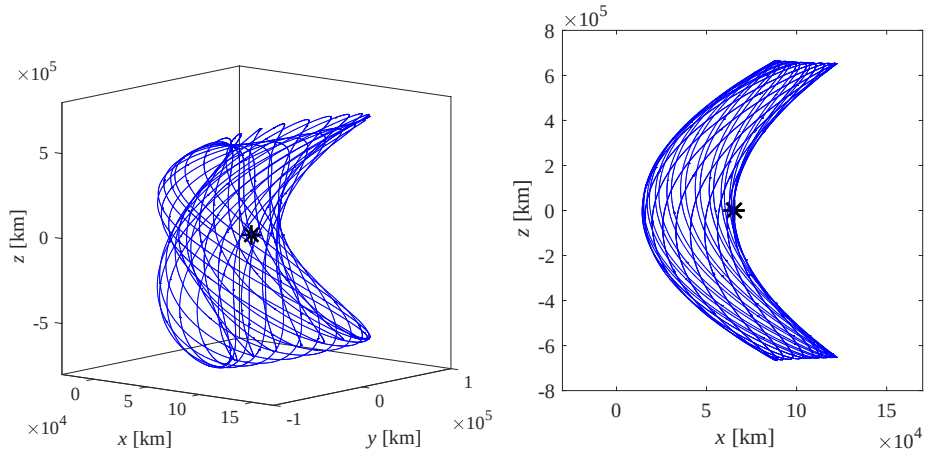

(a) 3-D view (b) projection onto x-z plane

Figure 2: Quasi-periodic orbit (quasi vertical Lyapunov orbit): $\boldsymbol{\xi} = [0.01, 0, 0, 0]^{\mathrm{T}}$. The initial positions are shown by asterisks.

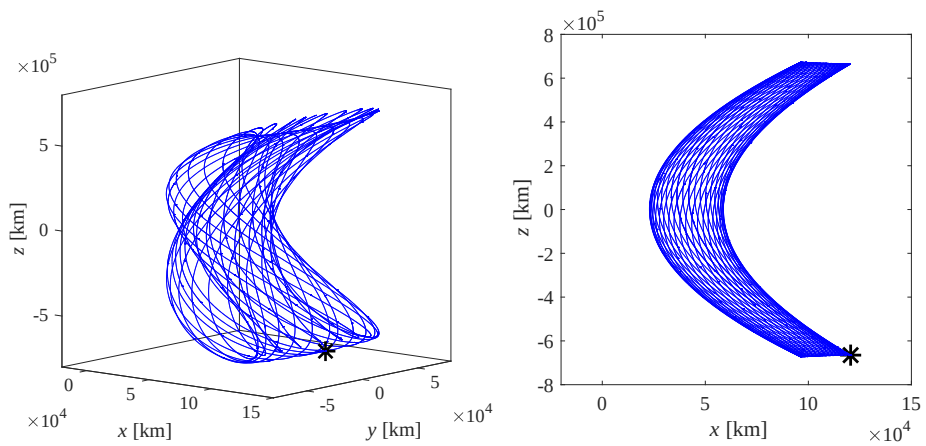

(a) 3-D view (b) projection onto x-z plane

Figure 3: Quasi-periodic orbit (quasi vertical Lyapunov orbit): $\boldsymbol{\xi} = [0, 0.01, 0, 0]^{\mathrm{T}}$. The initial positions are shown by asterisks.

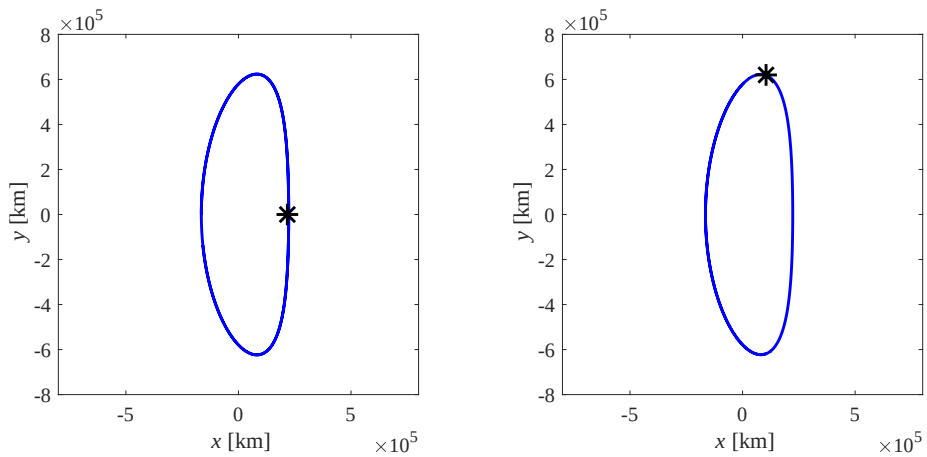

(a) $z_{c_3}(t_0) = 0.01$ and $z_{c_4}(t_0) = 0$

(b) $z_{c_3}(t_0) = 0$ and $z_{c_4}(t_0) = 0.01$

Figure 4: Periodic orbits (Lyapunov orbits): $\boldsymbol{\xi} = [0, 0, z_{c_3}(t_0), z_{c_4}(t_0)]^{\mathrm{T}}$. The initial positions are shown by asterisks.

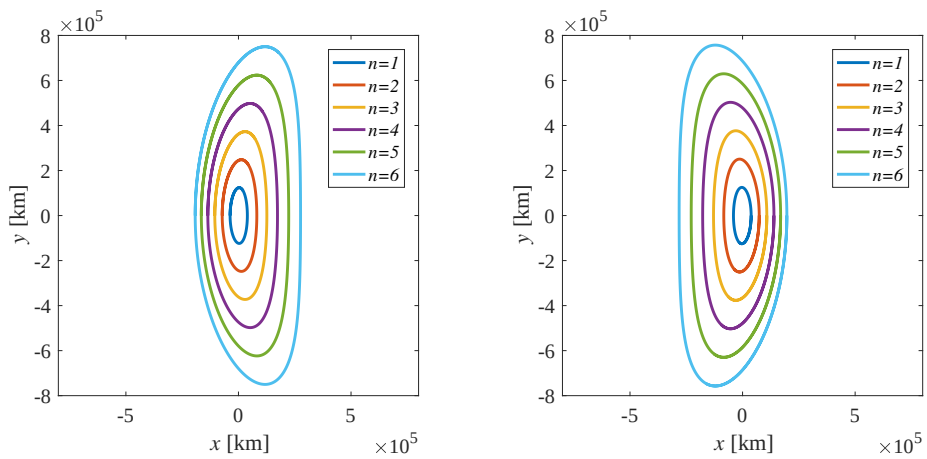

(a) L_1 Lyapunov Family

(b) L_2 Lyapunov Family

Figure 5: Lyapunov Family obtained by the center manifold design method.

4.2. Family of Lyapunov orbits

From the findings stated in Section 4.1, a Lyapunov orbit is found by a parameter vector

$$\boldsymbol{\xi}_{Lyapunov} = \begin{bmatrix} 0 & 0 & z_{c_3}(t_0) & z_{c_4}(t_0) \end{bmatrix}^{\mathrm{T}} \tag{28}$$

where at least one of $z_{c_3}(t_0)$ and $z_{c_4}(t_0)$ is nonzero. As examples, setting $z_{c4}(t_0) = 0$ and $z_{c3}(t_0) = 2n \times 10^{-3}$ $(n = 1, 2, \cdots, 6)$, the L_1 Lyapunov orbits and L_2 Lyapunov orbits are obtained by the center manifold design step, as shown in Fig. 5.

4.3. Finding vertical Lyapunov orbit from quasi-periodic orbit around L_1

For a vertical Lyapunov orbit, the initial parameter vector $\boldsymbol{\xi}$ is randomly chosen as

$$\boldsymbol{\xi} = \begin{bmatrix} 0 & 10 & 0 & 0 \end{bmatrix}^{\mathrm{T}} \times 10^{-3} \tag{29}$$

This parameter vector generates a quasi-periodic orbit, which is already drawn in Fig. 3. By setting a Poincaré section Σ to the x-y plane and the one-sided Poincaré map as $\boldsymbol{P}^+$ including only the intersections of the quasi-periodic orbit with Σ that have positive value of z', the discrete points on Σ fall on a closed curve. Therefore, the quasi-periodic orbit can be characterized by two periods: returning time T_r and winding time T_w. Let the returning time T_r be the average time taken for points starting from Σ to return back to it. That is,

$$T_r = \lim_{n\to\infty} \frac{1}{n} \sum_{i=1}^{n} (T_{i+1} - T_i) \tag{30}$$

where T_i is the discrete time obtained by the i-th iteration of $\boldsymbol{P}^+$. On the other hand, according to the literature [35], the winding time represents the average number of iterates of $\boldsymbol{P}^+$ required to return to $\boldsymbol{x}_0$. Let $\boldsymbol{P}_i$ be the discrete point obtained by the i-th iteration of $\boldsymbol{P}^+$, and assume that $\boldsymbol{P}_{i_k}$ passes over $\boldsymbol{P}_1$ after the discrete points move k times around the closed loop. Then, the winding time is defined by

$$T_w = \lim_{k\to\infty} \frac{i_k}{k} \tag{31}$$

However, it is impossible to compute exact T_r and T_w due to limits to infinity. In practice, it is necessary to truncate to some order to compute approximate T_r and T_w. Let $T_{r,n}$ and $T_{w,k}$ be the n-th and k-th terms of the limits, respectively. Then, we consider that $T_{r,n}$ and $T_{w,k}$ converge to T_r and T_w, respectively, when

$|T_{r,n} - T_{r,n+1}| < 10^-5$ and $|T_{w,k} - T_{w,k+1}| < 10^-2$ are satisfied. Then, the approximate returning time and winding time of the obtained quasi-periodic orbit are computed as $T_r = 3.1714$ and $T_w = 19.515$, respectively. The period of a periodic orbit that exists near quasi-periodic orbits seems to be close to the returning time of the quasi-periodic orbit. On the other hand, from the definition of the winding time, it approaches zero as the periodicity of the orbit increases. Therefore, the initial guess of the half-period of the periodic orbit for the differential correction step is set as one half of the returning time, i.e., $t_c = 1.5857$. Thus, the initial guess of the half-period of the periodic orbit for the differential correction step is set as one half of the returning time, i.e., $t_c = 1.5857$.

When the parameter vector is of the form $\boldsymbol{\xi} = \begin{bmatrix} 0 & z_{c_2}(t_0) & 0 & 0 \end{bmatrix}^{\mathrm{T}}$, purely periodic orbit never exists except for the case $z_{c_2}(t_0) = 0$; this is the libration point. Therefore, z_{c_2} is fixed and z_{c_3} is modified in the differential correction step as along with t_c. It should be noted that the quasi-vertical orbit drawn in Fig. 3 has small discontinuities at patch points because of the accumulation of numerical errors, but these discontinuities are very small and negligible in the differential correction step. In fact, there are 730 patch points in the quasi-vertical orbit drawn in Fig. 3, and the averaged position and velocity differences at the patch points are 1.1659×10^{-9} (174.42 m) and 3.7869×10^{-9} (1.1287×10^{-4} m/s), respectively. The initial set $(\boldsymbol{\xi}, t_c)$ is corrected by using Eq. (26), and after five iterations, it finally converges to

$$\boldsymbol{\xi} = \begin{bmatrix} 0 & 10 & -0.61160 & 0 \end{bmatrix}^{\mathrm{T}} \times 10^{-3}, \quad t_c = 1.5855 \tag{32}$$

This corrected set $(\boldsymbol{\xi}, t_c)$ forms an exact periodic orbit, which is the vertical Lyapunov orbit shown by the red line in Fig. 6. Note that the z-component after the differential correction step is the same as that of the quasi vertical Lyapunov orbit. This is because fixing z_{c_2} is equivalent to fixing z from Eq. (7).

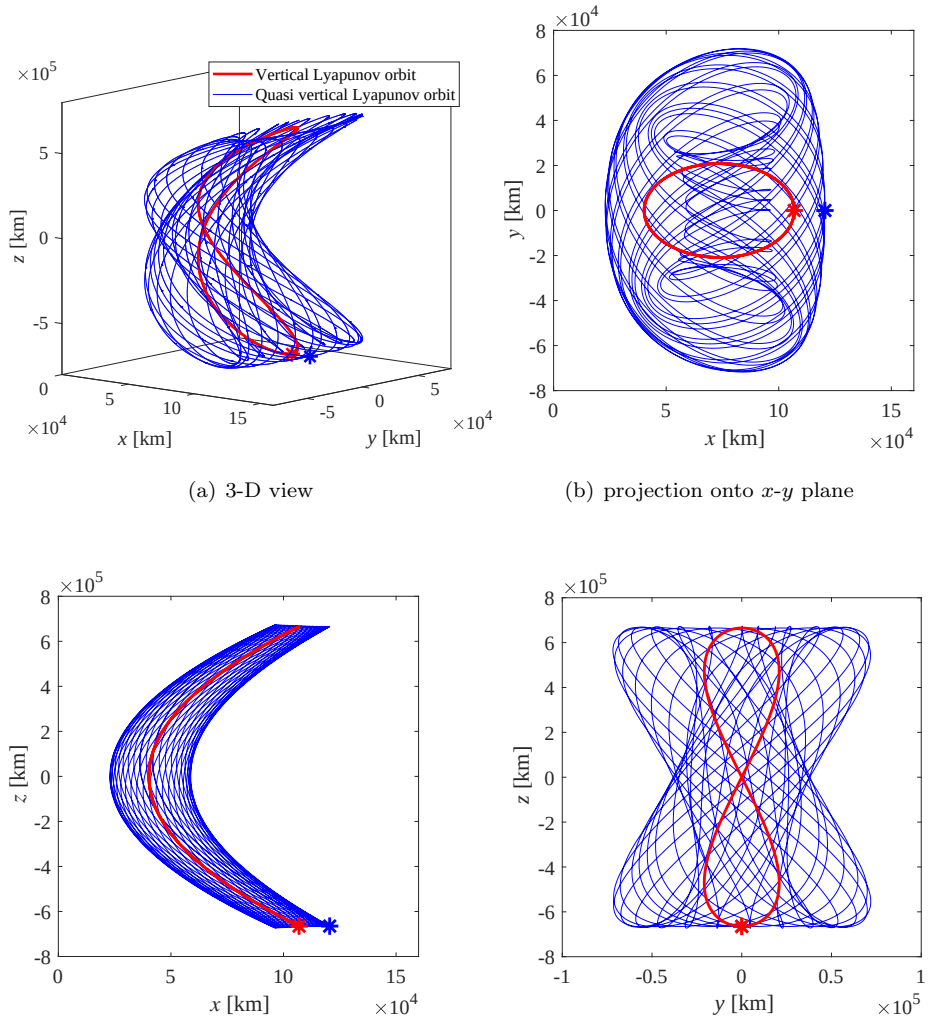

(a) 3-D view

(b) projection onto x-y plane

(c) projection onto x-z plane

(d) projection onto y-z plane

Figure 6: Periodic orbit obtained by differential correction step (z_{c_2}-fixed case). The blue and red orbits are obtained by the center manifold step and differential correction step, respectively. The initial positions are shown by asterisks.

4.4. Finding halo orbit from quasi-periodic orbit around L_2

Since the proposed method is applicable to any collinear libration point, a halo orbit around the L_2 point is now demonstrated. The initial parameter

vector $\boldsymbol{\xi}$ is randomly chosen as

$$\boldsymbol{\xi} = \begin{bmatrix} 0 & -5 & -11 & 0 \end{bmatrix}^{\mathrm{T}} \times 10^{-3} \tag{33}$$

This parameter vector generates a quasi-halo orbit, which is shown by blue lines in Figs. 7 and 8. By setting the Poincaré section to the x-y plane, the obtained quasi-periodic orbit is characterized by the approximate returning time $T_r = 3.1036$ and the winding time $T_w = 40.063$, and therefore the initial guess of the half-period of the periodic orbit is set as one half of the returning time, i.e., $t_c = 1.5518$. It should be noted that the obtained quasi-halo orbit has small discontinuities at patch points because of the accumulation of numerical errors, but these discontinuities are very small and negligible in the differential correction step.

First, z_{c_2} is fixed and z_{c_3} is modified in the differential correction step as along with t_c. The initial set $(\boldsymbol{\xi}, t_c)$ is corrected by Eq. (26), and after ten iterations, it finally converges to

$$\boldsymbol{\xi} = \begin{bmatrix} 0 & -5 & -12.688 & 0 \end{bmatrix}^{\mathrm{T}} \times 10^{-3}, \quad t_c = 1.5470 \tag{34}$$

This corrected set $(\boldsymbol{\xi}, t_c)$ forms an exact periodic orbit, which is the halo orbit shown by the red line in Fig. 7. Note that the z-component after the differential correction step is the same as that of the quasi-halo orbit.

Similarly, the set $(\boldsymbol{\xi}, t_c)$ can be corrected by Eq. (27), and after sixteen iterations, it converges to

$$\boldsymbol{\xi} = \begin{bmatrix} 0 & -1.8058 & -11 & 0 \end{bmatrix}^{\mathrm{T}} \times 10^{-3}, \quad t_c = 1.5511 \tag{35}$$

This corrected set $(\boldsymbol{\xi}, t_c)$ generates the halo orbit shown by the red line in Fig. 8. Note that unlike the z_{c_2}-fixed case, all the components of the initial position are slightly changed by the differential correction step. The reason for this is that fixing z_{c_3} does not mean fixing any components of the position vector but fixing the ratio of x and y' from Eq. (7).

Whereas the classical differential correction method cannot provide a quasi-periodic orbit, quasi-periodic orbits can be found by a simple procedure, and they can be modified to periodic orbits by the proposed method.

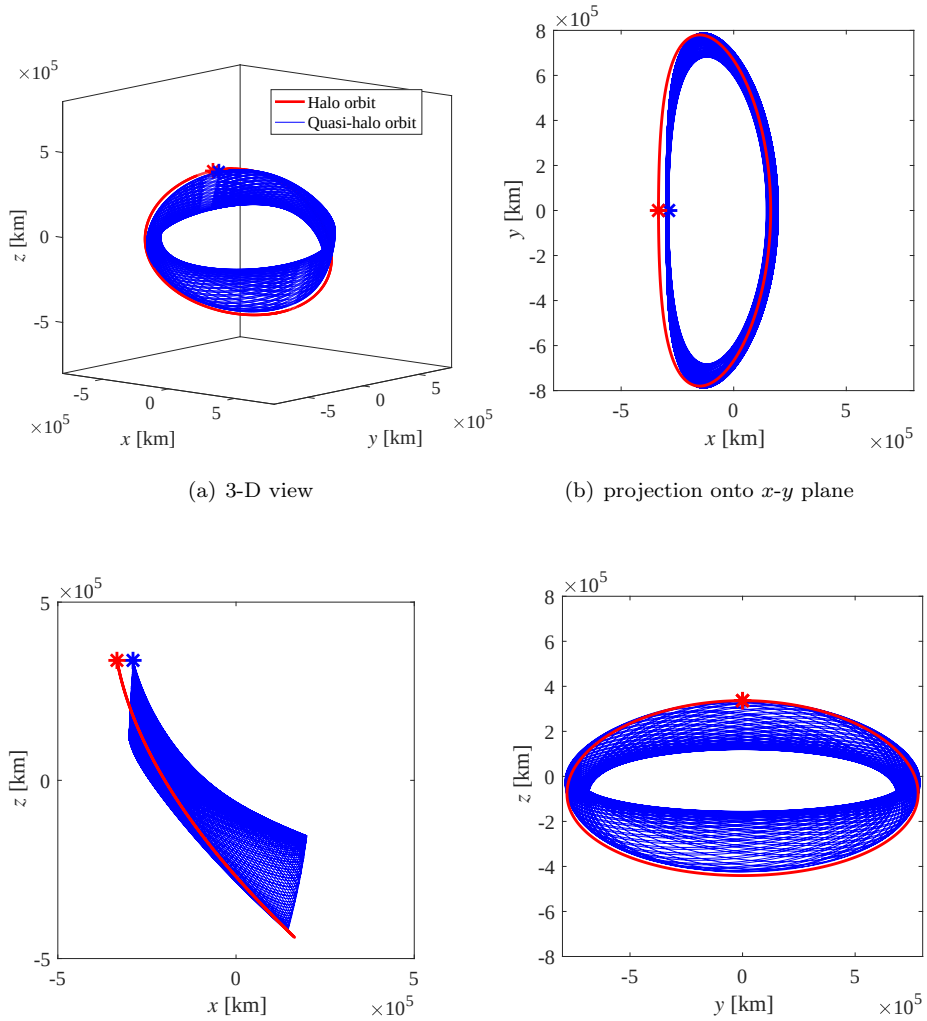

(a) 3-D view

(b) projection onto x-y plane

(c) projection onto x-z plane

(d) projection onto y-z plane

Figure 7: Periodic orbit obtained by differential correction step (z_{c_2}-fixed case). The blue and red orbits are obtained by the center manifold step and differential correction step, respectively. The initial positions are shown by asterisks.

5. Conclusion

A new numerical method for quasi-periodic and periodic orbits in the circular restricted three-body problem has been proposed based on the center manifold theory. The proposed method approximates the center manifold itself

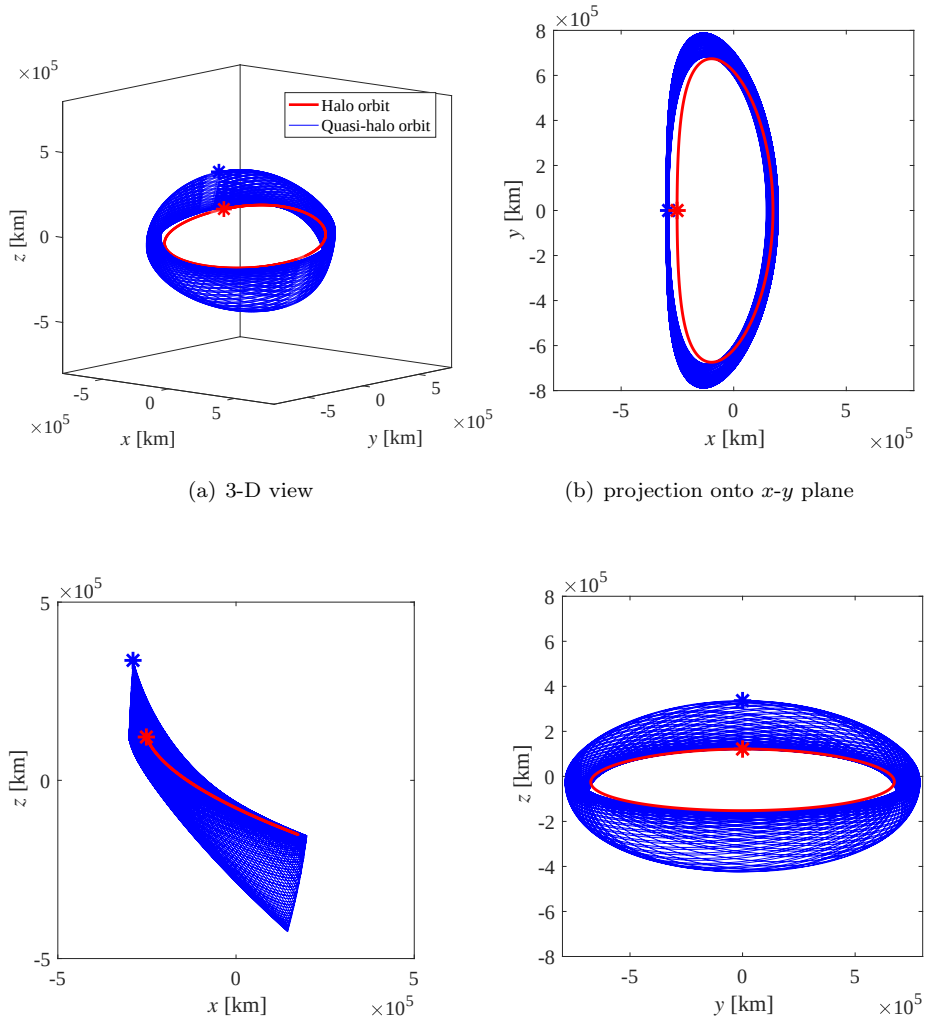

(a) 3-D view

(b) projection onto x-y plane

(c) projection onto x-z plane

(d) projection onto y-z plane

Figure 8: Periodic orbit by differential correction step (z_{c_3}-fixed case). The blue and red orbits are obtained by the center manifold step and differential correction step, respectively. The initial positions are shown by asterisks.

by defining a successive sequence that converges to the center manifold, and quasi-periodic and periodic orbits can be easily generated without an initial guess or extensive algebraic manipulations, which are necessary in conventional methods, being required. The proposed method includes two steps. The first

step is the center manifold design step, which yields quasi-periodic orbits and provides initial guesses for the correction step, and the second step is the differential correction step, which yields periodic orbits. Two different types of correction equations have been demonstrated in numerical simulations.

Appendix A. Transformation Matrix

The explicit expressions of the eigenvalues of matrix $\boldsymbol{T}$ are give by $\pm\lambda_{c_1}$, $\pm\lambda_{c_2}$, λ_s, and λ_u where

$$\begin{aligned} \lambda_{c_1} &= \Lambda_1 j, \quad \lambda_{c_2} = \Lambda_2 j \\ \lambda_s &= -\Lambda_3, \quad \lambda_u = \Lambda_3 \end{aligned}$$

and

$$\begin{aligned} \Lambda_1 &= \sqrt{\sigma_i} \\ \Lambda_2 &= \sqrt{\frac{\sqrt{\sigma_i(9\sigma_i - 8)}}{2} - \left(\frac{\sigma_i}{2} - 1\right)} \\ \Lambda_3 &= \sqrt{\frac{\sqrt{\sigma_i(9\sigma_i - 8)}}{2} + \left(\frac{\sigma_i}{2} - 1\right)} \end{aligned}$$

The matrix $\boldsymbol{A}$ can be transformed into the diaglonal form $\boldsymbol{D}$ by a transformation matrix $\boldsymbol{T}$

$$\boldsymbol{D} = \boldsymbol{T}^{-1}\boldsymbol{A}\boldsymbol{T} = \begin{bmatrix} \boldsymbol{P} & 0 & 0 \\ 0 & Q & 0 \\ 0 & 0 & R \end{bmatrix} \tag{A. 1}$$

where

$$\boldsymbol{P} = \begin{bmatrix} 0 & \Lambda_1 & 0 & 0 \\ -\Lambda_1 & 0 & 0 & 0 \\ 0 & 0 & 0 & \Lambda_2 \\ 0 & 0 & -\Lambda_2 & 0 \end{bmatrix}, \quad Q = -\Lambda_3, \quad R = \Lambda_3$$

The transformation matrix $\boldsymbol{T}$ is given by

$$\boldsymbol{T} = \begin{bmatrix} \mathrm{Re}(\boldsymbol{v}_{c_1}) & \mathrm{Im}(\boldsymbol{v}_{c_1}) & \mathrm{Re}(\boldsymbol{v}_{c_2}) & \mathrm{Im}(\boldsymbol{v}_{c_2}) & \boldsymbol{v}_s & \boldsymbol{v}_u \end{bmatrix} \tag{A. 2}$$

where

$$\boldsymbol{v}_{c_1} = \begin{bmatrix} 0 & 0 & -\dfrac{1}{\sqrt{1+\sigma_i}}j & 0 & 0 & \dfrac{\sqrt{\sigma_i}}{\sqrt{1+\sigma_i}} \end{bmatrix}^{\mathrm{T}} \tag{A. 3}$$

$$\boldsymbol{v}_{c_2} = \frac{1}{Q_2}\begin{bmatrix} \dfrac{1}{\Lambda_2} & -\dfrac{1}{d_2}j & 0 & j & \dfrac{\Lambda_2}{d_2} & 0 \end{bmatrix}^{\mathrm{T}} \tag{A. 4}$$

$$\boldsymbol{v}_s = \frac{1}{Q_3}\begin{bmatrix} -\dfrac{1}{\Lambda_3} & -\dfrac{1}{d_3} & 0 & 1 & \dfrac{\Lambda_3}{d_3} & 0 \end{bmatrix}^{\mathrm{T}} \tag{A. 5}$$

$$\boldsymbol{v}_u = \frac{1}{Q_3}\begin{bmatrix} -\dfrac{1}{\Lambda_3} & \dfrac{1}{d_3} & 0 & -1 & \dfrac{\Lambda_3}{d_3} & 0 \end{bmatrix}^{\mathrm{T}} \tag{A. 6}$$

and the quantities Q_i and d_i $(i = 2, 3)$ are defined as

$$Q_2 = \sqrt{\frac{1}{\Lambda_2^2} + \frac{1}{d_2^2} + 1 + \frac{\Lambda_2^2}{d_2^2}}$$

$$Q_3 = \sqrt{\frac{1}{\Lambda_3^2} + \frac{1}{d_3^2} + 1 + \frac{\Lambda_3^2}{d_3^2}}$$

$$d_2 = \frac{4(\sigma_i - 1)}{4 - 3\sigma_i - \sqrt{\sigma_i(9\sigma_i - 8)}}$$

$$d_3 = \frac{4(\sigma_i - 1)}{4 - 3\sigma_i + \sqrt{\sigma_i(9\sigma_i - 8)}}$$

Appendix B. Derivation of Eq. (24)

Consider the new variable $\boldsymbol{\alpha}(t) = \begin{bmatrix} \boldsymbol{z}^{\mathrm{T}}(t) & t_c \end{bmatrix}^{\mathrm{T}}$. The differentiation of $\boldsymbol{\alpha}(t)$ with respect to the non-dimensional time unit is

$$\boldsymbol{\alpha}'(t) = \boldsymbol{D}^*\boldsymbol{\alpha}(t) + \boldsymbol{g}^*(\boldsymbol{\alpha}(t)) \tag{B. 1}$$

where $\boldsymbol{D}^* = \mathrm{diag}\begin{bmatrix} \boldsymbol{D} & 0 \end{bmatrix}$ and $\boldsymbol{g}^*(\boldsymbol{\alpha}(t)) = \begin{bmatrix} \boldsymbol{g}(\boldsymbol{z}(t))^{\mathrm{T}} & 0 \end{bmatrix}^{\mathrm{T}}$. Let $\boldsymbol{\alpha}_n(t) = \begin{bmatrix} \boldsymbol{z}_n^{\mathrm{T}}(t) & t_{c,n} \end{bmatrix}^{\mathrm{T}}$ be the nominal variable and define the variation $\delta\boldsymbol{\alpha}(t) = \boldsymbol{\alpha}(t) - \boldsymbol{\alpha}_n(t)$. Then, the time derivative of the variation is computed as

$$\begin{aligned} \delta\boldsymbol{\alpha}'(t) &= \left(\boldsymbol{D}^* + \left.\frac{\partial \boldsymbol{g}^*(\boldsymbol{\alpha}(t))}{\partial \boldsymbol{\alpha}(t)}\right|_{\boldsymbol{\alpha}_n(t)}\right)\delta\boldsymbol{\alpha}(t) \\ &\triangleq \boldsymbol{W}^*(t)\delta\boldsymbol{\alpha}(t) \end{aligned} \tag{B. 2}$$

Therefore, the general solution is

$$\delta\boldsymbol{\alpha}(t) = \boldsymbol{\Phi}^*(t, t_0)\delta\boldsymbol{\alpha}(t_0) \tag{B. 3}$$

where STM $\boldsymbol{\Phi}^*$ satisfies $\boldsymbol{\Phi}^{*'}(t,t_0) = \boldsymbol{W}^*(t)\boldsymbol{\Phi}^*(t,t_0)$ and $\boldsymbol{\Phi}^*(t,t) = \boldsymbol{I}$. Since the STM $\boldsymbol{\Phi}^*(t,t_0)$ is defined as matrix partials, it is expressed as

$$\boldsymbol{\Phi}^*(t,t_0) = \frac{\partial \boldsymbol{\alpha}(t)}{\partial \boldsymbol{\alpha}(t_0)} = \begin{bmatrix} \boldsymbol{\Phi}(t,t_0) & \dfrac{\partial \boldsymbol{z}(t)}{\partial t_c} \\ \boldsymbol{0} & 1 \end{bmatrix} \tag{B. 4}$$

Then, substituting Eq. (B. 4) into Eq. (B. 3) yields

$$\begin{bmatrix} \delta \boldsymbol{z}(t) \\ \delta t_c \end{bmatrix} = \begin{bmatrix} \boldsymbol{\Phi}(t,t_0) & \dfrac{\partial \boldsymbol{z}(t)}{\partial t_c} \\ \boldsymbol{0} & 1 \end{bmatrix} \begin{bmatrix} \delta \boldsymbol{z}(t_0) \\ \delta t_c \end{bmatrix} \tag{B. 5}$$

Finally, resolving and evaluating Eq. (B. 5) at $t = t_c$ yields

$$\delta \boldsymbol{z}(t_c) = \begin{bmatrix} \boldsymbol{\Phi}(t_c,t_0) & \boldsymbol{z}'(t_c) \end{bmatrix} \begin{bmatrix} \delta \boldsymbol{z}(t_0) \\ \delta t_c \end{bmatrix} \tag{B. 6}$$

References

[1] R. W. Farquhar, Lunar communications with libration-point satellites., Journal of Spacecraft and Rockets 4 (10) (1967) 1383–1384. https://doi.org/10.2514/3.29095.

[2] R. W. Farquhar, A halo-orbit lunar station., Astronautics and Aeronautics 10 (6) (1972) 59–63.

[3] G. Gómez, J. Llibre, R. Martınez, C. Simó, Dynamics and Mission Design Near Libration Point Orbits–Volume 1: Fundamentals: The Case of Collinear Libration Points, World Scientific, London, 2001. https://doi.org/10.1142/4402.

[4] J. S. Parker, R. L. Anderson, Low-Energy Lunar Trajectory Design, John Wiley & Sons, 2014. https://www.doi.org/10.1002/9781118855065.

[5] C. D. Murray, S. F. Dermott, Solar System Dynamics, Cambridge university press, 1999. https://doi.org/10.1017/CBO9781139174817.

[6] J. E. Prussing, B. A. Conway, Orbital Mechanics, 2nd Edition, Oxford University Press, USA, New York, 2012.

[7] M. Hénon, Vertical stability of periodic orbits in the restricted problem. i. equal masses, Astronomy and Astrophysics 28 (1973) 415. https://doi.org/10.1007/bf01231427.

[8] K. C. Howell, Three-dimensional, periodic, 'halo' orbits, Celestial Mechanics and Dynamical Astronomy 32 (1) (1984) 53–71. https://doi.org/10.1007/bf01358403.

[9] J. V. Breakwell, J. V. Brown, The 'halo' family of 3-dimensional periodic orbits in the earth-moon restricted 3-body problem, Celestial Mechanics and Dynamical Astronomy 20 (4) (1979) 389–404. https://doi.org/10.1007/bf01230405.

[10] G. Gómez, J. Masdemont, C. Simó, Quasihalo orbits associated with libration points, Journal of the Astronautical Sciences 46 (2) (1998) 135–176.

[11] K. C. Howell, Families of orbits in the vicinity of the collinear libration points, Journal of the Astronautical Sciences 49 (1) (2001) 107–126. https://doi.org/10.2514/6.1998-4465.

[12] G. Gómez, J. Masdemont, J. Mondelo, Libration point orbits: A survey from the dynamical point of view (2003) 311–372. https://doi.org/10.1142/9789812704849_0016.

[13] B. G. Marchand, K. C. Howell, Control strategies for formation flight in the vicinity of the libration points, Journal of Guidance, Control, and Dynamics 28 (6) (2005) 1210–1219. https://doi.org/10.2514/1.11016.

[14] A. Héritier, K. C. Howell, Natural regions near the collinear libration points ideal for space observations with large formations, The Journal of the Astronautical Sciences 60 (1) (2013) 87–108. https://doi.org/10.1007/s40295-014-0027-8.

[15] D. L. Richardson, Analytic construction of periodic orbits about the collinear points, Celestial Mechanics and Dynamical Astronomy 22 (3) (1980) 241–253. https://doi.org/10.1007/bf01229511.

[16] K. C. Howell, H. J. Pernicka, Numerical determination of lissajous trajectories in the restricted three-body problem, Celestial Mechanics 41 (1-4) (1987) 107–124. https://doi.org/10.1007/bf01238756.

[17] E. Kolemen, N. J. Kasdin, P. Gurfil, Quasi-periodic orbits of the restricted three-body problem made easy, New Trends in Astrodynamics and Applications III(AIP Conference Proceedings Volume 886) 886 (2007) 68–77. https://doi.org/10.1063/1.2710044.

[18] Z. P. Olikara, K. C. Howell, Computation of quasi-periodic invariant tori in the restricted three-body problem, AAS 10-120 (2010) 1–15.

[19] Z. P. Olikara, D. J. Scheeres, Numerical method for computing quasi-periodic orbits and their stability in the restricted three-body problem, Advances in the Astronautical Sciences 145 (2012) 911–930.

[20] S. B. Broschart, G. Lantoine, D. J. Grebow, Quasi-terminator orbits near primitive bodies, Celestial Mechanics and Dynamical Astronomy 120 (2) (2014) 195–215. https://doi.org/10.1007/s10569-014-9574-3.

[21] N. Baresi, D. J. Scheeres, H. Schaub, Bounded relative orbits about asteroids for formation flying and applications, Acta Astronautica 123 (2016) 364–375. https://doi.org/10.1016/j.actaastro.2015.12.033.

[22] M. Ghorbani, N. Assadian, Optimal station-keeping near earth–moon collinear libration points using continuous and impulsive maneuvers, Advances in Space Research 52 (12) (2013) 2067–2079. https://doi.org/10.1016/j.asr.2013.09.021.

[23] M. Nazari, W. Anthony, E. A. Butcher, Continuous thrust stationkeeping in earth-moon l_1 halo orbits based on lqr control and floquet theory (2014) AIAA Paper 2014–4140. https://doi.org/10.2514/6.2014-4140.

[24] D. C. Folta, T. A. Pavlak, A. F. Haapala, K. C. Howell, M. A. Woodard, Earth–moon libration point orbit stationkeeping: theory, modeling, and

operations, Acta Astronautica 94 (1) (2014) 421–433. https://doi.org/10.1016/j.actaastro.2013.01.022.

[25] M. Zhu, H. R. Karimi, H. Zhang, Q. Gao, Y. Wang, Active disturbance rejection station-keeping control of unstable orbits around collinear libration points, Mathematical Problems in Engineering 2014 (2014) 1–14. https://doi.org/10.1155/2014/410989.

[26] C. E. Roberts, S. Case, J. Reagoso, Lissajous orbit control for the deep space climate observatory sun-earth l_1 libration point mission, AAS/AIAA Astrodynamics Specialist Conference AAS Paper 15-611 (2015) 1–20.

[27] M. Shirobokov, S. Trofimov, M. Ovchinnikov, Survey of station-keeping techniques for libration point orbits, Journal of Guidance, Control, and Dynamics 40 (2017) 1085–1105. https://doi.org/10.2514/1.g001850.

[28] Y. Akiyama, M. Bando, N. Hamidreza, S. Hokamoto, Trajectory design using the center manifold theory in the circular restricted three-body problem, 30th International Symposium on Space Technology and Science (2015).

[29] Y. Akiyama, M. Bando, N. Hamidreza, S. Hokamoto, Trajectory design using the center manifold theory in the circular restricted three-body problem, Transactions of the Japan Society for Aeronautical and Space Sciences, Aerospace Technology Japan (2016) Pd_151–Pd_158. https://doi.org/10.2322/tastj.14.pd_151.

[30] K. Nagata, N. Sakamoto, Y. Habaguchi, Center manifold method for the orbit design of the restricted three body problem, 2015 54th IEEE Conference on Decision and Control (CDC) (2015) 1769–1774. https://doi.org/10.1109/cdc.2015.7402466.

[31] H. Suzuki, N. Sakamoto, S. Celikovskỳ, Analytical approximation method for the center manifold in the nonlinear output regulation problem, 47th IEEE Conference on Decision and Control (2008) 1163–1168. https://doi.org/10.1109/cdc.2008.4738935.

[32] B. Wie, Space Vehicle Dynamics and Control, AIAA, 1998, pp. 282–285.

[33] H. Khalil, Nonlinear systems, Prentice Hall, 2001.

[34] L. Perko, Differential Equations and Dynamical Systems, Vol. 7, Springer Verlag, 2001, pp. 220–223.

[35] A. H. Nayfeh, B. Balachandran, Applied nonlinear dynamics: analytical, computational and experimental methods, John Wiley & Sons, 2008.